Performance simulation by a nonlinear thermodynamic model for a Free Piston Stirling Engine with a linear generator

Mahdi Majidniya, Thierry Boileau, Benjamin Rémy, Majid Zandi

Version of Record: https://www.sciencedirect.com/science/article/pii/S1359431120336085
Manuscript_ef8d7b54d88de47de6c799abd11b5996

Performance simulation by a nonlinear thermodynamic model for a Free Piston Stirling Engine with a Linear Generator

Mahdi MAJIDNIYA[1*], Thierry BOILEAU[1], Benjamin REMY[1], Majid ZANDI[2]

[1]Université de Lorraine, CNRS, LEMTA
F-54000 Nancy, France
[2] Renewable Energies Engineering Department, Shahid Beheshti University
Tehran, Iran
[*](Corresponding author: Mahdi.Majidniya@univ-lorraine.fr)

Abstract - In the present study, an RE-1000 Free Piston Stirling Engine (FPSE) combined with a Permanent Magnet Linear Synchronous Machine (PMLSM) was analyzed. First, a nonlinear thermodynamic model of the FPSE was developed and validated. Based on this model, gas temperatures and pressures in different parts of the system and also its thermal efficiency can be calculated. Then, the PMLSM was modeled. At the next step, the systems were combined, and the results of the adapted controlled combined system were presented. Finally, by modifying the reference velocity parameters (amplitude and frequency), respecting the physical limitations of the system, it is possible to find the optimum operating point. At this optimum operating point, the efficiency of the system is maximum. The results also showed that this optimum point happened when the summation of the pistons' strokes (power piston stroke + displacer piston stoke) was at its maximum amplitude.

Keywords: Free Piston Stirling Engine (FPSE); Permanent Magnet Linear Synchronous Machine (PMLSM); System Optimization; Nonlinear Thermodynamic simulation; Waste heat recovery; Microgrid

Nomenclature

A	Area, m^2	V	Volume, m^3
B_v	Friction coefficient	$\dot{W}$	Power, W
C	Clearance, m	x	Displacement, m
C_f	Darcy friction factor	$\dot{x}$	Velocity, m/s
Cp	Specific Heat in constant pressure, J/kgK	$\ddot{x}$	Acceleration, m/s^2
Cv	Specific Heat in constant volume, J/kgK	*Greek symbols*	
d	Diameter, m	γ	Specific heat ratio
$\underline{dh}$	Hydraulic diameter, m	θ	Angle
F	Force, N	μ	Dynamic viscosity, Pa.s
h	Convective heat transfer coefficient, W/kgK	ρ	Density, kg/m^3
i	Current, A	τ	Pole pitch, m
I	Inductance, mH	ψ_f	Flux linkage, Wb
K_i, K_p	Constant coefficients	ω	Angular velocity, rad/s
L	Length, m	*Index and exponent*	
m	Mass, kg	b	Buffer
$\dot{m}$	Mass flow rate, kg/s	c	Compression

P	Pressure, Pa	d	Displacer
Pr	Prandtl	dg	Displacer gas spring
$\dot{Q}$	Heat transfer, W	e	Expansion
R	Gas constant, J/kgK	el	Electric
r	Resistance, Ω	em	Electromagnetic
Re	Reynolds number	h	Heater
T	Temperature, K	k	Cooler
$\dot{T}$	Temperature variation in time, K/s	m	Mover
u	Velocity, m/s	p	Power piston
v	Voltage, V	R	Regenerator
		w	Wire

1. Introduction

Converting thermal energy to electricity is one of the most common energy conversions in the world. Generally, for each source of thermal energy, a system that can match to that source characteristics is developed, which should have a high efficiency.

Stirling engines are systems with one of the highest theoretical efficiencies. Due to their external combustion, they can work with many renewable or nonrenewable heat sources. These systems can work with different energy sources such as biomass, solar energy, natural gas, or gasoline [1]. Thus, these systems can be used in a large range of applications as a main thermal conversion system or as an auxiliary one for heat recovery purposes beside systems like fuel cells, data centers, automotive engines and different industrial processes (steel industry, chemistry industry, and other industries.) [2–6]. Stirling engines based on their generator type can be categorized into rotating and linear ones. In a rotating Stirling engine, the linear movement of the power piston is converted into a rotary one through a crank-shaft in order to be used in a rotating generator. In a linear Stirling engine, the linear movement of the power piston is converted to electricity directly through a linear generator. Furthermore, from the transmission mechanism point of view, a Stirling engine can be kinematic or dynamic. In the kinematic ones, the power piston and displacer piston are connected by a rigid connector. In the dynamic ones that are known as Free Piston Stirling Engines (FPSE) and were invented by W.T. Beale in 1964 [7], the pistons' movements are synchronized by their dynamic behavior. An FPSE combined with a Permanent Magnet Linear Synchronous Machine (PMLSM) compared to conventional power generators has a higher efficiency cost ratio [1,8]. Moreover, they are reliable systems that, compared to the rotating ones, are more compact, lightweight, and have better sealing [8–10]. In order to develop tools that can help the design and also the use of the FPSE-PMLSM system, an accurate model with an adapted control system is required. All of these drew the attention of the authors to this topic.

Tavakolpour-Saleh et al. [11,12] described new FPSE designing methods (multiple-scale perturbation and genetic algorithm). The results showed more than a 20% difference between theoretical and experimental power production. It should be noted that they ignored the losses including pressure drops inside heat exchangers. They used a linearized set of equations in their studies by ignoring nonlinear terms. de la Bat et al. [13] studied an FPSE by a fully explicit one-dimensional model based on the linearized equations. Comparing theoretical and experimental results showed a big difference between calculated and measured space

pressures and output power. Many reasons can cause this problem, including ignoring losses such as pressure drops. Ye et al. [14], based on a linearized model of a beta-type FPSE while ignoring the pressure drops, and also known sinusoidal movements of the pistons, studied the effect of the dynamic input parameters on the FPSE. They had a huge difference between numerical and experimental phase angles that as they mentioned, is due to ignore the pressure drops in heat exchangers. Chi et al. [15] developed a two-dimensional axisymmetric CFD model for beta-type FPSE. The results show more than a 30% difference between theoretical and experimental power output. As they mentioned, this difference can be due to some FPSE losses that were neglected.

The knowledge of the pressure drops is a key parameter to have a good estimation of FPSE behavior [16]. The best way to estimate the pressure drops is to use the equations which are closer to reality. This goal can be achieved by nonlinear equations. Also using a thermodynamic model by providing the instantaneous gas properties in each part of the system, gives the information which is useful to have a more precise estimation of the system behavior including its efficiency [17]

Based on the bibliography that has been done by the authors, a detailed nonlinear thermodynamic study of the FPSE combined with a linear generator has not been done yet. Most of the recent studies focused only on developing a linear alternator for the FPSE and did not present a model for it. They developed different linear generators to be coupled with an FPSE [18–23]. Some of the other studies just developed a linear model of the FPSE and focused on its dynamic aspects and did not present a model for the linear alternator [24,25]. They considered the generator as a damper for the FPSE. A few studies that modeled both systems did not go further than a linear model [26,27]. First of all, to develop a reliable controller for the FPSE-PMLSM combined system, an accurate model of both is needed.

All these come to this point that developing a precise combined model of an FPSE with a PMLSM is necessary. Furthermore, a linear model is not capable of predicting the realistic dynamic behavior of the FPSE [1]; thus, a nonlinear model is required. Also, Since the FPSE is a dynamic Stirling engine that the displacer piston and the power piston movements are synchronized by their dynamic behavior, and this behavior is a function of the pressures in the compression, expansion, buffer and gas spring spaces, a precise thermodynamic model, is needed to identify these thermodynamic values (pressures, temperatures, volumes, and other thermodynamic properties.). Also, in order to have a stable combined system, an adapted control system should be developed [13]. This adapted control system should ensure the stability of the system under different working conditions in order to be able to track the optimum operating point.

The first important point is that the present nonlinear thermodynamic model of the FPSE, which is coupled with a PMLSM, has not been done before as it is done in the present study (based on the bibliography that has been done by the authors). The next important point is that this study is presenting a new control method for the system. All the recent studies were based on the conventional PI (Proportional-Integral) or PID (Proportional-Integral-Derivative) controllers, but here, the conventional controllers are replaced with PR (Proportional-Resonant) controllers. For the present system, using a PR controller results in a wider range of stability, which allows us to find the optimum point of the system by varying the reference velocity amplitude and frequency. Finally, the effect of reference velocity parameters on the system was studied. Afterward, based on the physical limitations, the system based on the reference velocity parameters was optimized, which has not been done before. It should be noted that all the models were done in MATLAB Simulink®. This study is a foundation for an experimental one that will be done in the near future.

2. System Analysis

The schematic of the combined FPSE-PMLSM system is shown in Figure 1. The FPSE is a Sunpower RE-1000 engine, and the PMLSM is a three-phase alternator. The piston of the FPSE is connected to the PLMLSM mover, and their movements are controlling by a control system. The details of each system will be discussed in the following.

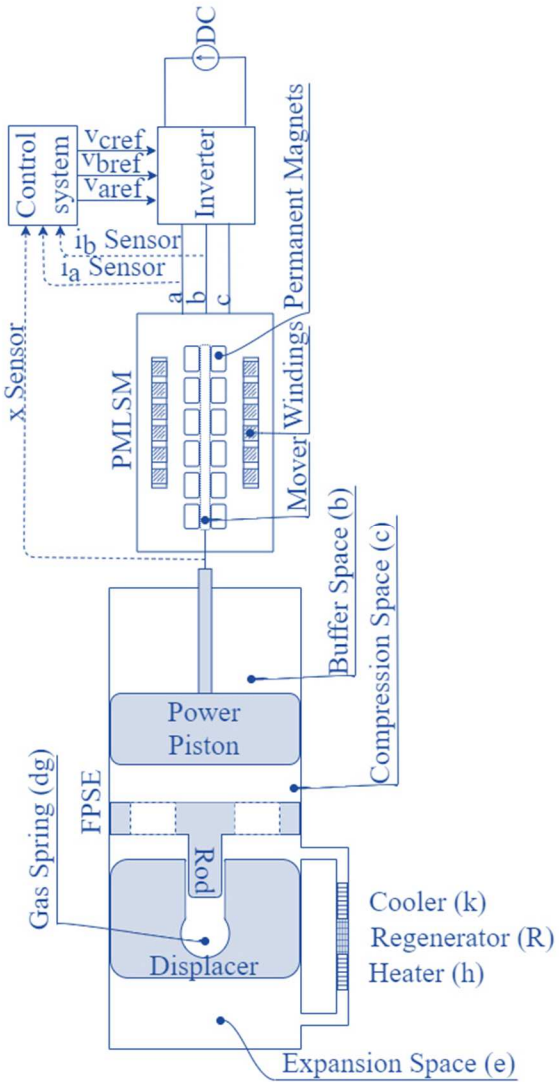

Figure 1: FPSE-PMLSM schematic

2.1. FPSE Analysis

The method that was used to develop the thermodynamic model of the FPSE is explained step by step in Table 1 with the related equations and descriptions. This model was developed in MATLAB Simulink®. It should be noted that in order to have a more precise model, the regenerator was divided into two parts ($R1, R2$),

Table 1: FPSE step by step modeling [1,17,28,29]

1	Input parameters/Initial values	
2	$\dot{V} = \dot{V}_c - \dot{V}_e = A_p\dot{x}_p - (2A_d - A_{rod})\dot{x}_d$	Instantaneous gas velocities

3	$u_i = \dot{V} / A_i \;\; ; i = k, h, R1, R2$	(u_i) in the heat exchangers based on the total gas volume flow rate ($\dot{V}$) through them
4	$\mu_i = 3.674 \times 10^{-7} T_i^{0.7} \;\; ; i = k, h, R1, R2$	
5	$Re_i = \rho_i u_i \underline{\underline{dh}}_i / \mu_i \;\; ; i = k, h, R1, R2$	
6	$V_c = A_p(x_p + C_c) - (A_d - A_{rod})x_d$	
7	$V_e = A_d(x_d + C_e)$	
8	$V_{avT} = \frac{A_p C_c}{T_k} + \frac{A_d C_e}{T_h} + \frac{V_h}{T_h} + \frac{V_k}{T_k} + \frac{V_R}{T_R}$	
9	$P_c = \frac{m_{total} R}{V_{avT}}$	
10	$\Delta P_i = \frac{1}{2}\rho_i \left(\frac{C_{fi} L_i}{\underline{\underline{dh}}_i}\right) u_i \lvert u_i \rvert \;\; ; i = k, h, R1, R2$	

C_{fi} can be calculated based on the following table:

For the heater and the cooler:	$Re < 2000$	$C_f = 64/Re$
	$Re > 2000$	$C_f = 0.316 Re^{-0.25}$
For the regenerator:	$Re < 60$	$C_f = 4 \times 10^{(1.73 - 0.93 \log Re)}$
	$60 < Re < 1000$	$C_f = 4 \times 10^{(0.714 - 0.365 \log Re)}$
	$Re > 1000$	$C_f = 4 \times 10^{(0.015 - 0.125 \log Re)}$

11	$P_k = P_c + \frac{\Delta P_k}{2}$	
12	$P_{R1} = P_k + \frac{\Delta P_k}{2} + \frac{\Delta P_{R1}}{2}$	
13	$P_{R2} = P_{R1} + \frac{\Delta P_{R1}}{2} + \frac{\Delta P_{R2}}{2}$	
14	$P_h = P_{R2} + \frac{\Delta P_{R2}}{2} + \frac{\Delta P_h}{2}$	
15	$P_e = P_h + \frac{\Delta P_h}{2}$	
16	$\rho_i = \frac{48.14 P_i \times 10^{-5}}{T_i(1 + 0.4446 P_i \times 10^{-5} / T_i^{1.2})} \;\; ; i = k, h, R1, R2$	

After calculating the correct values of ρ_i, step 5 to 16 will be repeated.

17	$P_b = P_{mean}\left(\frac{V_{mean\,b}}{V_b}\right)^{\gamma} = P_{mean}\left(\frac{V_{mean\,b}}{V_{mean\,b} - A_p x_p}\right)^{\gamma}$	Based on the adiabatic assumptions

18	$P_{dg} = P_{mean}\left(\frac{V_{mean\,dg}}{V_{dg}}\right)^{\gamma} = P_{mean}\left(\frac{V_{mean\,dg}}{V_{mean\,dg} - A_{rod}x_d}\right)^{\gamma}$	for buffer and displacer gas spring
19	$\Delta P = \Delta P_k + \Delta P_{R1} + \Delta P_{R2} + \Delta P_h$	
20	$\ddot{x}_p = \left(A_p(P_c - P_b) - F_{load}\right)/m_p$	
21	$\ddot{x}_d = \left(A_d P_e - (A_{dg} - A_{rod})P_c - A_{rod}(P_{dg})\right)/m_d$ $= \left(A_d(P_e - P_c) + A_{rod}(P_c - P_{dg})\right)/m_d$ $= \left(A_d \Delta P + A_{rod}(P_c - P_{dg})\right)/m_d$	
Integrating of $\ddot{x}_p$ and $\ddot{x}_d$ will result in $\dot{x}_p$, $\dot{x}_d$, x_p, and x_d that will be used as input parameters (Step 1)		
22	$m_i = \frac{\rho_i}{V_i}\ ; i = k, h, R1, R2$	
After calculating m_i, by a derivation, $\dot{m}_i$ values will be calculated that will be used as input parameters (Step 1)		
23	$\dot{m}_{k\ to\ c} = -\dot{m}_{c\ to\ k} = \dot{m}_c$	$\dot{m}_{i\ to\ j}$ is the mass flow rate from space i to space j
24	$\dot{m}_{R1\ to\ k} = -\dot{m}_{k\ to\ R1} = \dot{m}_c + \dot{m}_k$	
25	$\dot{m}_{R2\ to\ R1} = \dot{m}_c + \dot{m}_k + \dot{m}_{R1}$	
26	$\dot{m}_{h\ to\ e} = -\dot{m}_{e\ to\ h} = \dot{m}_e$	
27	$\dot{m}_{R2\ to\ h} = -\dot{m}_{h\ to\ R2} = \dot{m}_e + \dot{m}_h$	
28	$\dot{m}_{R1\ to\ R2} = \dot{m}_e + \dot{m}_h + \dot{m}_{R2}$	
29	$\dot{m}_{i\ to\ j} > 0 \Rightarrow T_{ij} = T_{ji} = T_i \quad else \quad T_{ij} = T_{ji} = T_j$	
30	$Pr_i = \frac{0.7117 \times T_i^{-\left(0.01 - 1.42\times10^{-4}\times P_i \times 10^{-5}\right)}}{1 + 1.123 \times 10^{-3} \times P_i \times 10^{-5}}\ ; i = k, h, R1, R2$	
31	$h_i = \frac{C_{fi}}{4} \times \frac{Re_i \mu_i Cp}{2\underline{dh}_i Pr_i}\ ; i = k, h, R1, R2$	
32	$\dot{Q}_i = h_i A_{wetted\ i}(T_{wall\ i} - T_i)\ ; i = k, h, R1, R2$	
33	$\dot{T}_c = \left(\left(\dot{m}_{k\ to\ c} CpT_{kc} - \dot{W}_p\right)/Cv - \dot{m}_c T_c\right)/m_c$	
34	$\dot{T}_k = \left(\left(\dot{Q}_k + \dot{m}_{c\ to\ k} CpT_{ck} + \dot{m}_{R1\ to\ k} CpT_{R1k}\right)/Cv - \dot{m}_k T_k\right)/m_k$	
35	$\dot{T}_{R1} = \left(\left(\dot{Q}_{R1} + \dot{m}_{k\ to\ R1} CpT_{kR1} + \dot{m}_{R2\ to\ R1} CpT_{R2R1}\right)/Cv - \dot{m}_{R1} T_{R1}\right)/m_{R1}$	
36	$\dot{T}_{R2} = \left(\left(\dot{Q}_{R2} + \dot{m}_{R1\ to\ R2} CpT_{R1R2} + \dot{m}_{h\ to\ R2} CpT_{hR2}\right)/Cv - \dot{m}_{R2} T_{R2}\right)/m_{R2}$	
37	$\dot{T}_h = \left(\left(\dot{Q}_h + \dot{m}_{R2\ to\ h} CpT_{R2h} + \dot{m}_{e\ to\ h} CpT_{eh}\right)/Cv - \dot{m}_h T_h\right)/m_h$	
38	$\dot{T}_e = \left(\left(\dot{m}_{h\ to\ e} CpT_{he} - \dot{W}_d\right)/Cv - \dot{m}_e T_e\right)/m_e$	
After calculating $\dot{T}_i$, by an integration, T_i values will be calculated that will be used as input parameters (Step 1). These set of equations (33-38) are based on the following equation:		

$$\dot{Q}_{in} + \left(\dot{m}C_pT\right)_{in} - \left(\dot{m}C_pT\right)_{out} - \dot{W}_{out} = C_v \frac{d}{dt}(mT)$$

In Table 1, the whole procedure of the nonlinear thermodynamic FPSE modeling was described in detail, and all the equations were presented in the order that they have been utilized to model the system. As can be seen, the procedure of modeling is a step by step procedure that will start based on some assumptions, and after calculating the new values, they will be used as inputs for the next time step. The proposed model was also validated with experimental results of RE-1000 in Table 2. All the input parameters for the model validation are based on Schreiber [30] study.

Table 2: FPSE thermodynamic model validation

	Power (W)	Frequency (Hz)	Phase Shift (°)	Stroke_p (cm)	Stroke_d (cm)	Stroke ratio ($\boldsymbol{Stroke_d/Stroke_p}$)	Efficiency (%)
Exp. [30]	1000	30.2	47.6	2.32	2.55	1.099	27.4
Theoretical	1003.9	28.57	32.94	2.746	2.379	0.866	30.02
Error (%)	0.39	5.4	30.8	18.4	6.7	20.55	9.56

The piston stroke means the distance that the piston is travelling during a cycle. As can be seen, the thermodynamic model of FPSE was validated. Now, this model can be used in the combined system.

2.2. PMLSM Analysis

As it was discussed, a three-phase permanent magnet linear alternator was chosen to be coupled with the FPSE model. The set of equations that were used to model this system are as following:

$$v_d = I_d \frac{di_d}{dt} + ri_d - \frac{\pi}{\tau}\dot{x}I_q i_q \tag{2.2.1}$$

$$v_q = I_q \frac{di_q}{dt} + ri_q + \frac{\pi}{\tau}\dot{x}\left(I_d i_d + \sqrt{3/2}\,\psi_f\right) \tag{2.2.2}$$

$$F_{em} = \frac{\pi}{\tau}\left(\sqrt{3/2}\,\psi_f i_q + \left(I_d - I_q\right) i_d i_q\right) \tag{2.2.3}$$

$$m_m\ddot{x} = F_{em} - B_v\dot{x} - F_{load} \tag{2.2.4}$$

$$\dot{W}_{em} = F_{em}\dot{x} \tag{2.2.5}$$

$$\dot{W}_{el} = v_q i_q + v_d i_d \tag{2.2.6}$$

Since controlling the PMLSM in the three-phase frame $(a-b-c)$ is hard, the equations were written in the two-phase frame $(d-q)$. Converting three-phase to two-phase frames and vice versa can be done by Park and Concordia transformations [31].

$$\begin{bmatrix} Y_\alpha \\ Y_\beta \end{bmatrix} = \sqrt{\frac{2}{3}} \begin{bmatrix} 1 & -1/2 & -1/2 \\ 0 & \sqrt{3}/2 & -\sqrt{3}/2 \end{bmatrix} \begin{bmatrix} Y_a \\ Y_b \\ Y_c \end{bmatrix} \tag{2.2.7}$$

$$\begin{bmatrix} Y_d \\ Y_q \end{bmatrix} = \begin{bmatrix} \cos\theta & \sin\theta \\ -\sin\theta & \cos\theta \end{bmatrix} \begin{bmatrix} Y_\alpha \\ Y_\beta \end{bmatrix} \tag{2.2.8}$$

$$\begin{bmatrix} Y_\alpha \\ Y_\beta \end{bmatrix} = \begin{bmatrix} \cos\theta & -\sin\theta \\ \sin\theta & \cos\theta \end{bmatrix} \begin{bmatrix} Y_d \\ Y_q \end{bmatrix} \tag{2.2.9}$$

$$\begin{bmatrix} Y_a \\ Y_b \\ Y_c \end{bmatrix} = \sqrt{\frac{2}{3}} \begin{bmatrix} 1 & 0 \\ -1/2 & \sqrt{3}/2 \\ -1/2 & -\sqrt{3}/2 \end{bmatrix} \begin{bmatrix} Y_\alpha \\ Y_\beta \end{bmatrix} \tag{2.2.10}$$

Y is representing current (i)/voltage (v), and θ can be calculated as:

$$\theta = \int \frac{\pi}{\tau} \dot{x}\, dt \tag{2.2.11}$$

$\dot{x}$ is the speed of the PMLSM mover. Based on all these equations, the block diagram of the PMLSM model will be as Figure 2:

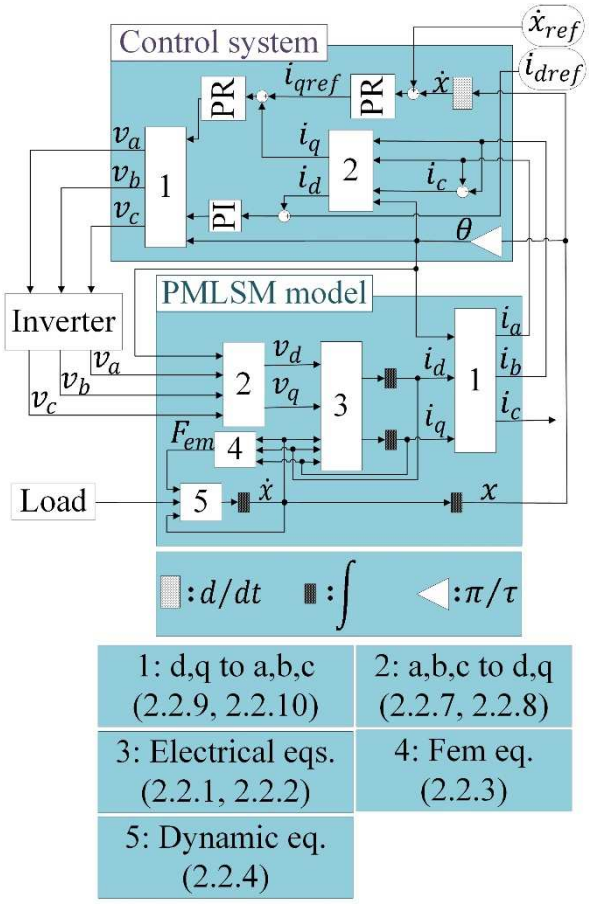

Figure 2: PMLSM block diagram

As can be seen, the model of the PMLSM was coupled with a control system to control it. In the control system, two PR (Proportional-Resonant) controllers to control i_q and $\dot{x}$ and one PI (Proportional- Integral) controller to control i_d are used. Using PR controllers results in a more stable system in a wider range of control/system parameter variations compared to PI controllers. The transfer functions of the PI and PR controllers are as:

$$PR: K_p + K_i \frac{0.4\omega S}{S^2 + 2\omega S + \omega^2} \tag{2.3.2}$$

$$PI: K_p + K_i \frac{1}{S} \tag{2.3.3}$$

2.3. Combined System Analysis

Coupling FPSE with PMLSM means coupling all the related equations together. To do this, since the PMLSM mover is connected to the FPSE power piston, their velocity and acceleration will be the same; thus in the PMLSM equations $\dot{x}$ will be replaced with $\dot{x}_p$. Furthermore, the dynamic equation of the PMLSM will be coupled with the dynamic equation of the FPSE power piston as:

$$\ddot{x}_p = \left(A_p(P_c - P_b) + F_{em} - B_v\dot{x}_p\right)/\left(m_p + m_m\right) \tag{2.3.1}$$

By making these changes in the PMLSM and FPSE set of equations, two systems can be coupled in MATLAB Simulink®. The input parameters of the combined system are presented in Table 3. The working gas is Helium.

Table 3: Combined system input parameters[1,30]

FPSE input parameters		d_{rod}	1.663 cm	$V_{mean\,b}$	2615 cm^3
$T_{wall\,h}$	814.3 K	d_h	0.2362 cm	$V_{mean\,d}$	37.97 cm^3
$T_{wall\,k}$	322.8 K	d_w	0.00889 cm	$V_{R1,R2}$	28.185 cm^3
$T_{wall\,R1}$	418.4 K	L_k	7.92 cm	$A_{wetted\,k}$	115.2 cm^2
$T_{wall\,R2}$	622.7 K	L_h	18.34 cm	PMLSM input parameters	
P_{mean}	71 bars	L_R	6.44 cm	r	0.1 Ω
$Porosity$	75.9 %	A_h	1.4898 cm^2	I_d	1.77 mH
m_d	0.426 kg	A_k	2.6163 cm^2	I_q	3.01 mH
m_p	6.2 kg	$A_{R1,R2}$	8.745 cm^2	ψ_f	0.0513 Wb
d_p	5.718 cm	C_c	1.83 cm	B_v	10
d_d	5.67 cm	C_e	1.861 cm	m_m	0.824 kg

Based on the input parameters of Table 3, the results of the combined system modeling are presented in Figure 3 - Figure 6. The reference value of i_d is equal to zero and for the velocity, the reference is a sinusoidal wave with an amplitude of 1.5 m/s and frequency of 30 Hz. Furthermore, the reference value of i_q is a result of controlling the velocity and its reference value.

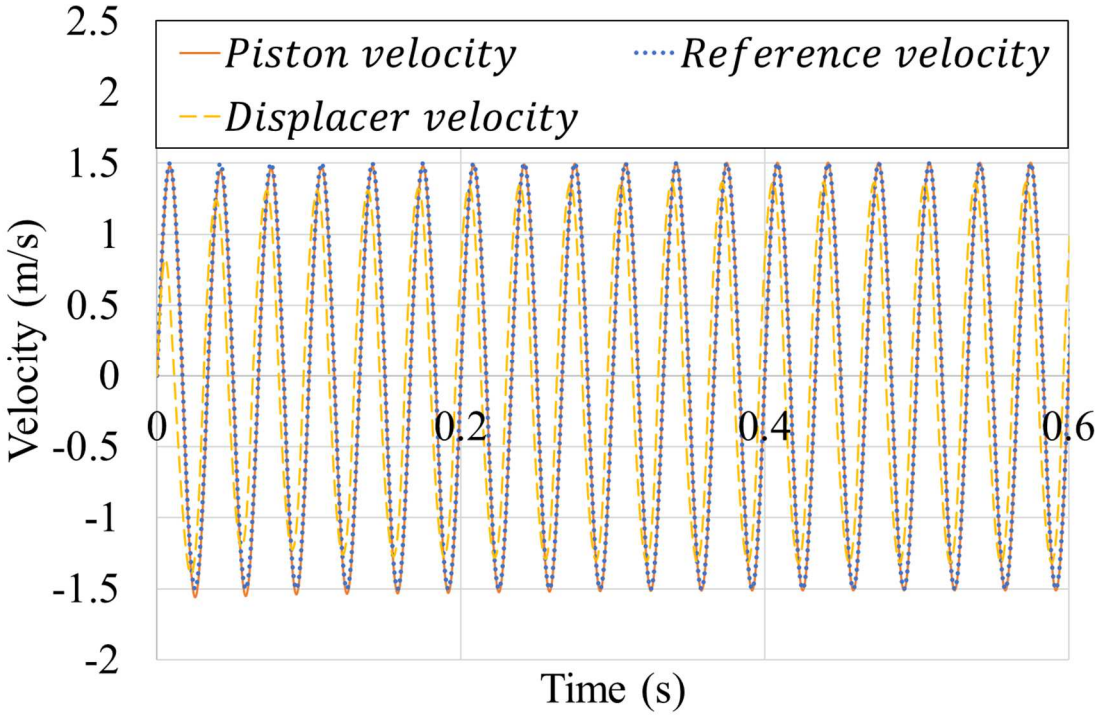

Figure 3: Variations of velocities

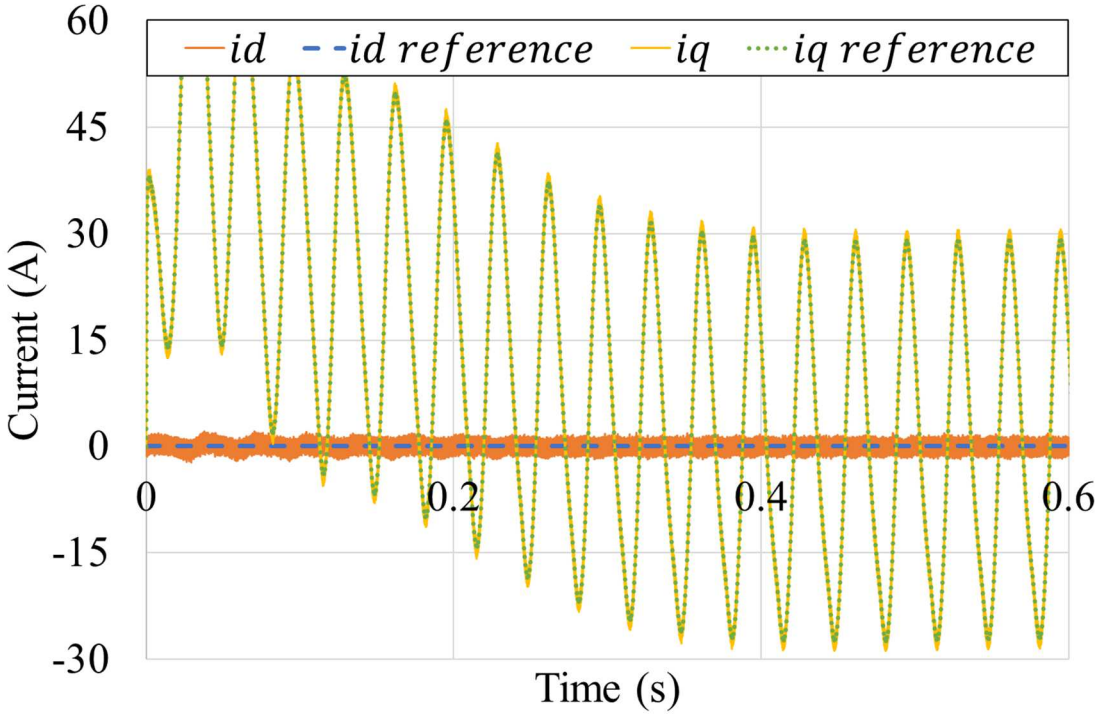

Figure 4: Variations of currents

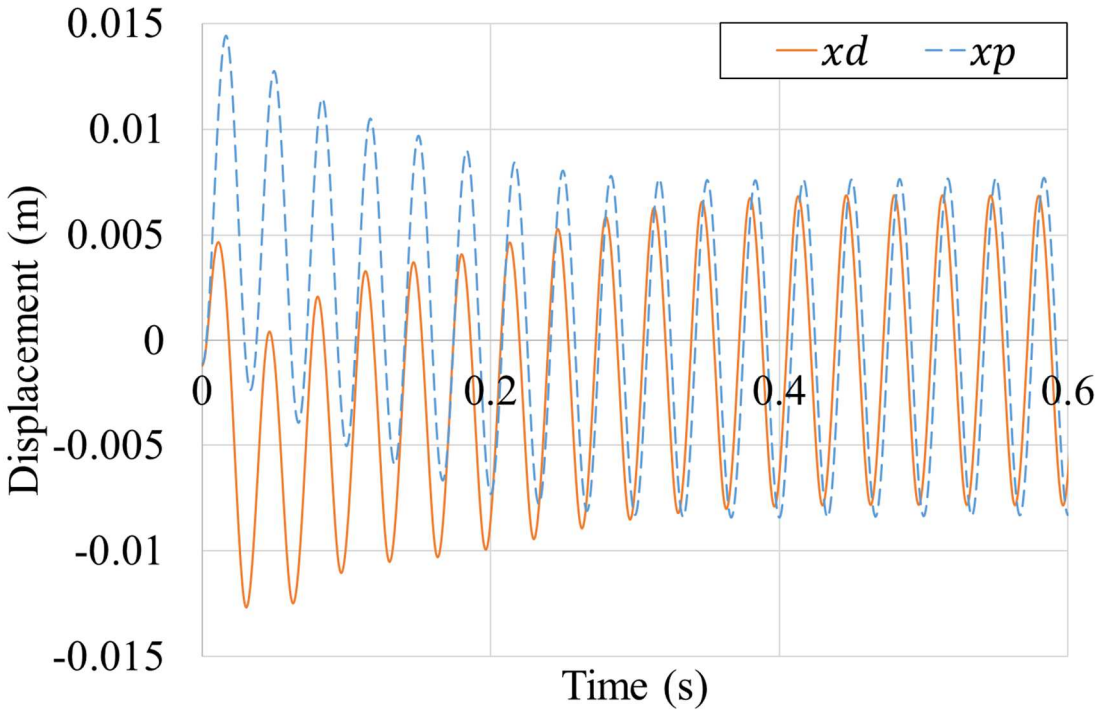

Figure 5: Variations of displacements

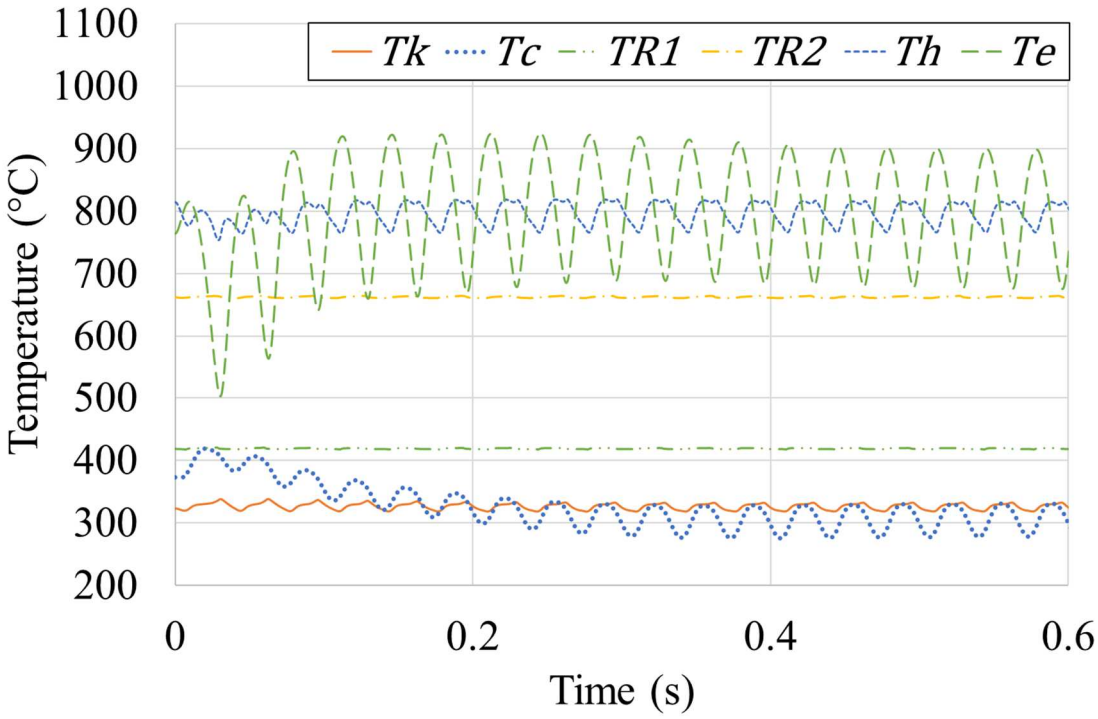

Figure 6: Variations of temperatures

Figure 3 and Figure 4 show the results of the system control. As can be seen, the combined system is well controlled, and always the resulted values follow their references. Figure 5 shows the power piston and displacer piston positions at each moment. As can be seen, after stabilization, the behavior of the system is almost sinusoidal. Figure 6 shows the gas temperature variation in each space. The regenerator temperatures are almost constant, but for other spaces, there is a periodic temperature variation. The maximum temperature variations

happen in expansion space. Based on all figures, it can be seen by having constant wall temperatures as Table 3 and having the same values as initial gas temperatures for step 1 of Table 1, the system will be stabilized just after a few cycles (less than 10 cycles).

2.4. System optimization

In this section, the effect of reference velocity parameters on the system, by considering its physical limitations, will be discussed. The physical limitations here are the maximum pistons' displacements that were identified during FPSE construction. The reference velocity parameters that here are reference velocity amplitude and frequency, directly affect the pistons' strokes. To study the effect of these parameters on the system and find out how the system can be optimized, the effect of each parameter separately and also simultaneously on the system performance was studied.

It is assumed that the maximum displacer and power piston strokes are 0.0154 m and 0.014 m, respectively.

First, variations of system parameters based on the reference velocity frequency at its constant amplitude, according to the system physical limitations, are studied. In Figure 7, it is shown that how increasing the velocity frequency at a constant amplitude of 1 $m \cdot s^{-1}$, will change the system behavior.

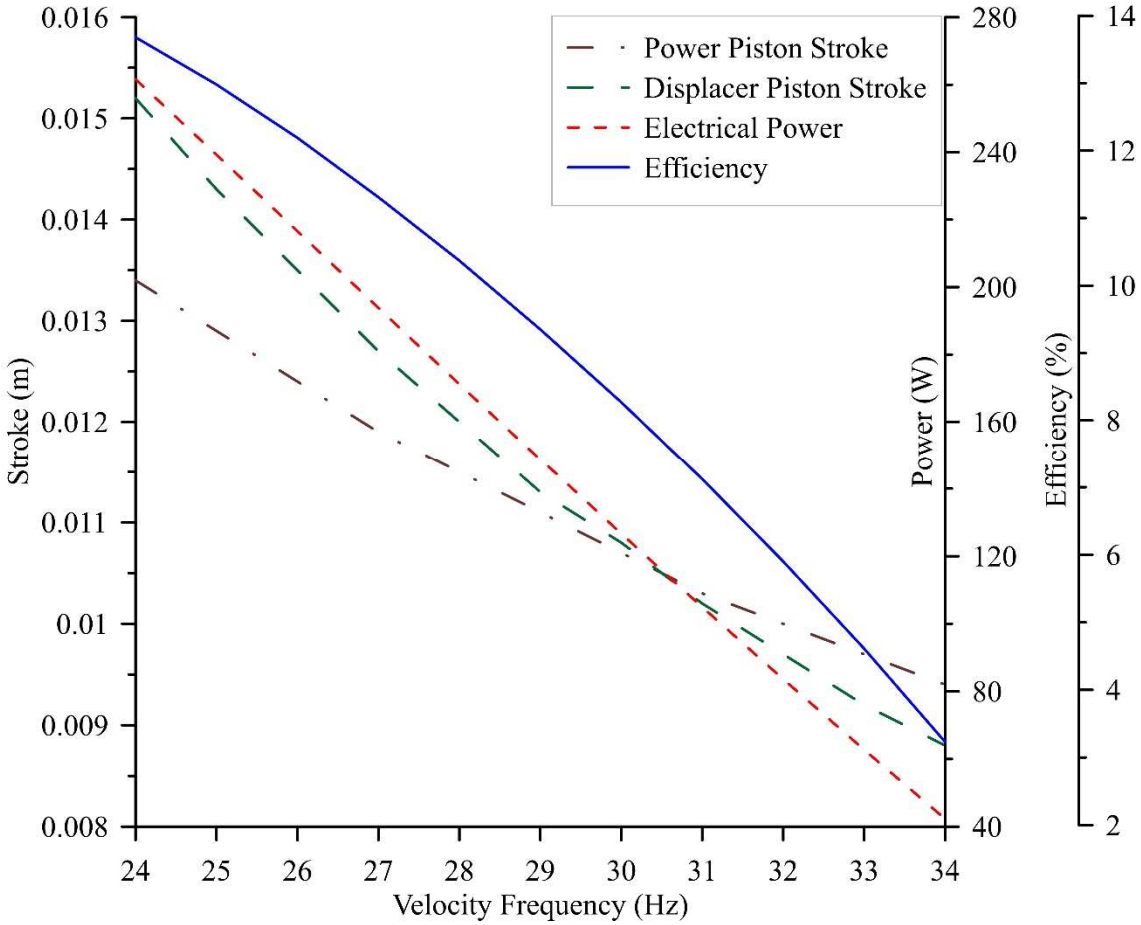

Figure 7: System results at reference variable velocity frequency and constant amplitude of 1 $\frac{m}{s}$

As can be seen in Figure 7, by increasing the reference velocity frequency at constant amplitude, the strokes of the pistons will decrease that cause decrement in electrical power and system efficiency. It means, at constant reference velocity amplitude, its frequency should

be as small as possible according to the physical limitations of the system. Here, in the frequency less than 24 Hz, the stroke of the power piston would get larger than its limit value, so more frequency decrements at this velocity amplitude are not possible.

In the next step, it is assumed that the reference velocity frequency will be constant at 24 Hz; and its amplitude will vary. This frequency was chosen based on Figure 7 because, at this frequency, the efficiency of the system is maximum. The results of this analysis are shown in Figure 8.

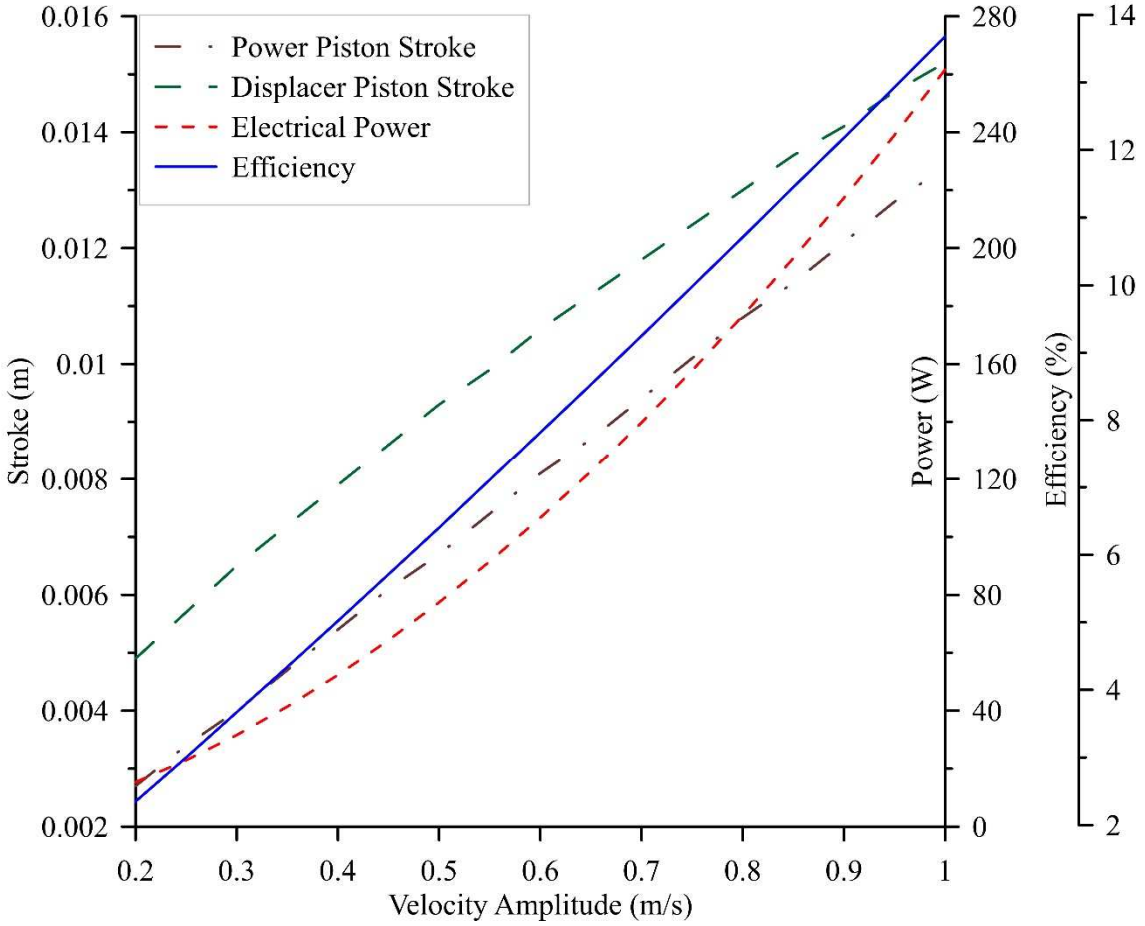

Figure 8: System results at variable velocity amplitude and constant frequency of 24 Hz

As can be seen, by increasing the reference velocity amplitude at a constant frequency, the pistons' strokes, and also the electrical power and the system efficiency, will increase. The results show that at a constant frequency, the reference velocity amplitude should be increased as much as possible.

As it was shown in Figure 7 and Figure 8, as much as the strokes of the pistons are higher, the system performance will be better. Therefore, the best working conditions based on these results could be the conditions that the pistons are at their maximum possible strokes. Since the pistons' strokes are increasing either by increasing the reference velocity amplitude or by decreasing the reference velocity frequency, there will be a lot of amplitude-frequency pairs that will result in the maximum stroke limit of a piston. Thus, when this stroke is needed to be at its maximum possible value to have the best performance of the system, many combinations of the amplitude-frequency pairs will give this maximum stroke. Necessarily, all these combinations are not the best possible solution for the system. In order to have an optimized system, the effect of each frequency-amplitude pair that results in the maximum strokes should be studied and compared to gain the best system operating condition. In Figure

9, the effect of different reference velocity amplitude-frequency pairs on the system efficiency is shown.

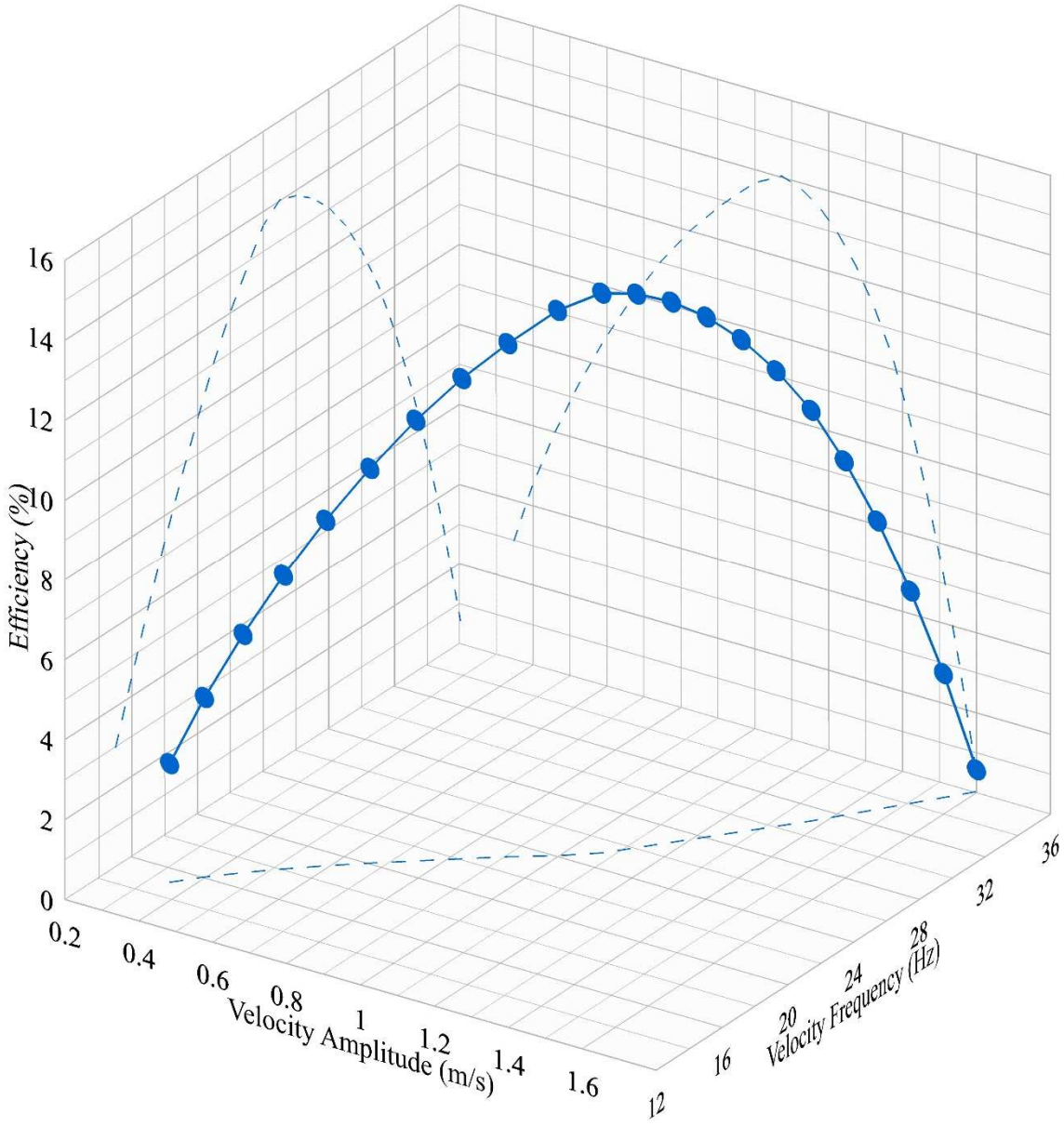

Figure 9: Efficiency variations at different reference velocity amplitude-frequency pairs for maximum strokes

As can be seen in Figure 9, by increasing the reference velocity amplitude and frequency, the efficiency will increase to a point and then starts to decrease. It means even at the maximum piston stroke, all the amplitude-frequency pairs do not have the same results, and one of these pairs is the optimal solution of the system. This optimal solution is a reference velocity with amplitude and frequency of 1.075 $m \cdot s^{-1}$ and 25 Hz, respectively that results in 14.05% of efficiency. This result is for the present case, with the assumed maximum displacer and power piston strokes of 0.0154 m and 0.014 m, respectively. It will be discussed that why this pair (1.075 $m \cdot s^{-1}$, 25 Hz) gives the maximum efficiency and the best performance of the system.

When it was said that these pairs were based on physical limitations, it means that at least one of the pistons reaches its maximum limit, and its stroke cannot be increased more, while another piston may not be at its maximum stroke. As it was shown in Figure 7 and Figure 8,

by changing the frequency and amplitude, both pistons' strokes have the same behavior and will increase/decrease at the same time. However, one of them will get to its maximum limit first, which will not allow more variations of the amplitude/frequency. Here it is the same case. When the amplitude-frequency pairs were calculated to have the maximum strokes, only the stroke of the piston that gets faster to its maximum limit was important, and the amplitude-frequency pairs were calculated based on that. It means with these pairs, at least one of the pistons gets to its physical limit.

Now to have an idea of why the amplitude-frequency pair of (1.075 $m \cdot s^{-1}$, 25 Hz) gives the maximum efficiency and the best performance of the system, the variations of pistons' strokes based on amplitude-frequency pairs of Figure 9 are shown in Figure 10. To have a better sense of this matter, the ratios of pistons' strokes at each pair of amplitude-frequency to their physical limit and summation of these two values are shown in Figure 10.

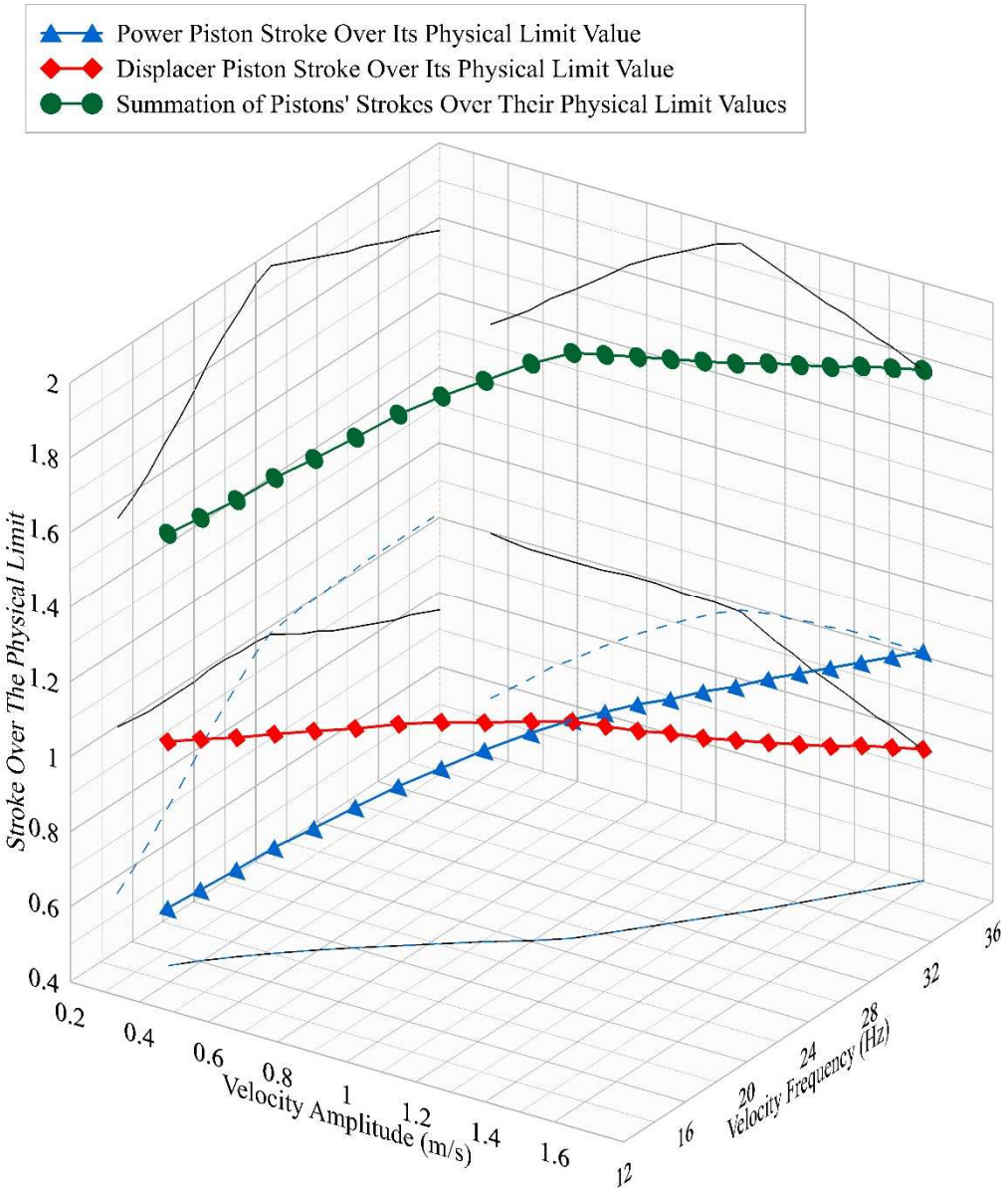

Figure 10: Ratios of piston strokes over their physical limit at different velocity amplitude-frequency pairs

As can be seen in Figure 10, first, the ratio of the displacer piston stroke over its maximum possible value is equal to 1, while the power piston stroke is smaller than its physical limit

value. At a point by increasing the reference velocity frequency and amplitude, the ratio of the power piston stroke over its maximum possible value will increase to 1, and the ratio of the displacer piston stroke to its limit will start to decrease. The summation of these two values is also shown in Figure 10. The maximum of summations happens exactly at the optimal point that was already achieved (1.075 $m \cdot s^{-1}$, 25 Hz). Now it can be understood that why this point is the optimal point. At this point, both power piston and displacer piston strokes, and not just one of them, have their maximum possible values. Thus, for such a system, it cannot be concluded that since the power piston is connected to the PMLSM mover, so its amplitude is the most and only important parameter that should be increased to have the best performance of the system. However, both power piston and displacer piston should have a high stroke to gain an optimized performance of the system. As can be seen in Figure 10, as much as pistons' strokes ratio to their maximum possible values are closer to each other, the system performance is better, and as much as they are getting far from each other, the performance of the system is getting worse.

3. Conclusion

The present study was developed in two main parts. The first part was about developing a nonlinear thermodynamic model of a Sunpower RE-1000 Stirling engine (β type Free Piston Stirling Engine). After validating this system, an electrodynamic model of a three-phase Permanent Magnet Linear Synchronous Machine was developed and coupled with it. Then the combined FPSE-PMLSM system was controlled with two PR (Proportional Resonant) controllers for velocity and i_q and one PI (Proportional Integrator) controller for i_d, and the results were shown.

In the second part, the system based on the reference velocity parameters was optimized. To achieve this goal, first, the effect of each reference velocity parameter (reference velocity amplitude and frequency) based on the physical limitations of the system (displacer piston and power piston maximum possible strokes) was studied. The results showed that by increasing the reference velocity amplitude or decreasing the reference velocity frequency, the strokes of pistons would increase, and as a result, the performance of the system will improve. Thus, the best solution for the reference velocity parameters were the parameters that give the maximum amplitude of strokes concerning their limitations. Therefore, the reference velocity amplitude-frequency pairs that gave the maximum strokes were calculated, and based on the efficiency at each pair, the optimized operating point of the system was extracted. For these pairs, first, by increasing the frequency and amplitude of the reference velocity, the efficiency of the system increased until it got to its maximum value. Then, increasing the frequency and amplitude of the reference velocity resulted in the efficiency decrement. The reason that why this point was the optimum point was also discussed based on the pistons' strokes at each point. The results show that as much as the summation of the ratio of pistons' strokes over their maximum possible values is higher, the system performance is better. In future studies, these reference velocity parameters will be tested on an experimental setup.

References

[1] M. Majidniya, T. Boileau, B. Remy, M. Zandi, Nonlinear modeling of a Free Piston Stirling Engine combined with a Permanent Magnet Linear Synchronous Machine, Appl. Therm. Eng. 165 (2020) 114544. https://doi.org/https://doi.org/10.1016/j.applthermaleng.2019.114544.

[2] M. Güven, H. Bedir, G. Anlaş, Optimization and application of Stirling engine for waste heat recovery from a heavy-duty truck engine, Energy Convers. Manag. 180 (2019) 411–424. https://doi.org/https://doi.org/10.1016/j.enconman.2018.10.096.

[3] M. Marefati, M. Mehrpooya, S.A. Mousavi, Introducing an integrated SOFC, linear Fresnel solar field, Stirling engine and steam turbine combined cooling, heating and power process, Int. J. Hydrogen Energy. 44 (2019) 30256–30279. https://doi.org/https://doi.org/10.1016/j.ijhydene.2019.09.074.

[4] A. Salehi, S.M. Mousavi, A. Fasihfar, M. Ravanbakhsh, Energy, exergy, and environmental (3E) assessments of an integrated molten carbonate fuel cell (MCFC), Stirling engine and organic Rankine cycle (ORC) cogeneration system fed by a biomass-fueled gasifier, Int. J. Hydrogen Energy. 44 (2019) 31488–31505. https://doi.org/https://doi.org/10.1016/j.ijhydene.2019.10.038.

[5] A.C. Ferreira, J. Silva, S. Teixeira, J.C. Teixeira, S.A. Nebra, Assessment of the Stirling engine performance comparing two renewable energy sources: Solar energy and biomass, Renew. Energy. 154 (2020) 581–597. https://doi.org/https://doi.org/10.1016/j.renene.2020.03.020.

[6] Z. Song, J. Chen, L. Yang, Heat transfer enhancement in tubular heater of Stirling engine for waste heat recovery from flue gas using steel wool, Appl. Therm. Eng. 87 (2015) 499–504. https://doi.org/https://doi.org/10.1016/j.applthermaleng.2015.05.028.

[7] G. Walker, Stirling engines, (1980).

[8] J. Subramanian, G. Heiskell, F. Mahmudzadeh, P. Famouri, Study of radial and axial magnets for linear alternator—Free piston engine system, in: Power Symp. (NAPS), 2017 North Am., IEEE, 2017: pp. 1–6.

[9] R. Redlich, A summary of twenty years experience with linear motors and alternators, Sunpower Inc. (1995).

[10] E.Y. Loktionov, A.A. Martirosyan, M.D. Shcherbina, Solar powered free-piston stirling—Linear alternator module for the lunar base, in: Ind. Eng. Appl. Manuf. (ICIEAM), Int. Conf., IEEE, 2016: pp. 1–6.

[11] A.R. Tavakolpour-Saleh, S. Zare, A. Omidvar, Applying perturbation technique to analysis of a free piston Stirling engine possessing nonlinear springs, Appl. Energy. 183 (2016) 526–541. https://doi.org/10.1016/j.apenergy.2016.09.009.

[12] S.H. Zare, A.R. Tavakolpour-Saleh, Frequency-based design of a free piston Stirling engine using genetic algorithm, Energy. 109 (2016) 466–480.

[13] B.J.G. de la Bat, R.T. Dobson, T.M. Harms, A.J. Bell, Simulation, manufacture and experimental validation of a novel single-acting free-piston Stirling engine electric generator, Appl. Energy. 263 (2020) 114585. https://doi.org/10.1016/j.apenergy.2020.114585.

[14] W. Ye, X. Wang, Y. Liu, Application of artificial neural network for predicting the dynamic performance of a free piston Stirling engine, Energy. 194 (2020) 116912. https://doi.org/10.1016/j.energy.2020.116912.

[15] C. Chi, J. Mou, M. Lin, G. Hong, CFD simulation and investigation on the operating mechanism of a beta-type free piston Stirling engine, Appl. Therm. Eng. 166 (2020). https://doi.org/10.1016/j.applthermaleng.2019.114751.

[16] F. Formosa, Coupled thermodynamic-dynamic semi-analytical model of free piston Stirling engines, Energy Convers. Manag. 52 (2011) 2098–2109. https://doi.org/10.1016/j.enconman.2010.12.014.

[17] I. Urieli, D.M. Berchowitz, Stirling cycle engine analysis, A. Hilger Bristol, 1984.

[18] T.T. Dang, P. François, L. Prévond, H. Ben Ahmed, Theoretical and experimental results of tubular linear induction generator for Stirling cogenerator system, in: XIX Int. Conf. Electr. Mach. 2010, IEEE, 2010: pp. 1–7.

[19] T.T. Dang, M. Ruellan, L. Prévond, H. Ben Ahmed, B. Multon, Sizing Optimization of Tubular Linear Induction Generator and Its Possible Application in High Acceleration Free-Piston Stirling Microcogeneration, IEEE Trans. Ind. Appl. 51 (2015) 3716–3733.

[20] T.T. Dang, M. Ruellan, H. Ben Ahmed, L. Prevond, B. Multon, Sizing optimization of tubular linear induction generator for a new stirling micro-cogenerator system, in: Power Electron. Electr. Drives, Autom. Motion (SPEEDAM), 2014 Int. Symp., IEEE, 2014: pp. 1362–1367.

[21] J.-M. Kim, J.-Y. Choi, K.-S. Lee, S.-H. Lee, Design and analysis of linear oscillatory single-phase permanent magnet generator for free-piston stirling engine systems, AIP Adv. 7 (2017) 56667.

[22] P. Zheng, B. Yu, S. Zhu, Q. Gong, J. Liu, Research on control strategy of free-piston stirling-engine linear-generator system, in: Electr. Mach. Syst. (ICEMS), 2014 17th Int. Conf., IEEE, 2014: pp. 2300–2304.

[23] W.P. Hew, J. Jamaludin, M. Tadjuddin, K.M. Nor, Fabrication and testing of linear electric generator for use with a free-piston engine, in: Power Eng. Conf. 2003. PECon 2003. Proceedings. Natl., IEEE, 2003: pp. 277–282.

[24] H. Karabulut, M. Okur, A.O. Ozdemir, Performance prediction of a Martini type of Stirling engine, Energy Convers. Manag. 179 (2019) 1–12.

[25] J. Boucher, F. Lanzetta, P. Nika, Optimization of a dual free piston Stirling engine, Appl. Therm. Eng. 27 (2007) 802–811.

[26] P. Zheng, C. Tong, J. Bai, B. Yu, Y. Sui, W. Shi, Electromagnetic design and control strategy of an axially magnetized permanent-magnet linear alternator for free-piston stirling engines, IEEE Trans. Ind. Appl. 48 (2012) 2230–2239.

[27] S. Zhu, G. Yu, O. Jongmin, T. Xu, Z. Wu, W. Dai, E. Luo, Modeling and experimental investigation of a free-piston Stirling engine-based micro-combined heat and power system, Appl. Energy. 226 (2018) 522–533.

[28] M. Majidniya, T. Boileau, R. Benjamin, M. Zandi, Thermoelectric modeling of a Free Piston Stirling Engine (FPSE) combined with a Permanent Magnet Linear Synchronous Machine (PMLSM) with its control system, in: Int. Conf. Renew. Energy Distrib. Gener. Iran, 2019.

[29] M. Majidniya, T. Boileau, R. Benjamin, M. Zandi, Modélisation thermo-électrique d'un moteur Stirling à piston libre et d'une machine synchrone linéaire à aimant permanent avec sa commande, in: Congrès Annu. La Société Française Therm., 2019.

[30] J. Schreiber, Testing and performance characteristics of a 1-kW free piston Stirling engine, (1983).

[31] G. Remy, Commande optimisée d'un actionneur linéaire synchrone pour un axe de positionnement rapide, (2007).